Kinetics and Mechanism of the Acid Transition of the Active Site in Plastocyanin†

Mathias A. S. Hass,‡ Hans E. M. Christensen,§ Jingdong Zhang,§ and Jens J. Led*,‡

Department of Chemistry, University of Copenhagen, Universitetsparken 5, DK-2100 Copenhagen Ø, Denmark, and Chemistry Department, The Technical University of Denmark, Building 207, DK-2800 Lyngby, Denmark

Received July 22, 2007; Revised Manuscript Received October 9, 2007

ABSTRACT: Exchange on the microsecond time scale between the protonated and deprotonated forms of His92 in the copper site of reduced plastocyanin from the cyanobacteria *Anabaena variabilis* was monitored using ^{15}N NMR relaxation measurements. On the basis of the dependence of the kinetics on pH and phosphate buffer concentration, we propose a two-step model for the protonation of the copper site in agreement with previous crystallographic studies. It is shown that the proton transfer is the rate-limiting step in the reaction at low buffer concentrations, whereas at high buffer concentrations, another step becomes rate-limiting. We suggest that the latter step is a concerted dissociation of His92 from the Cu(I) ion and a 180° rotation of the imidazole ring, which precede the protonation. The first-order rate constant for the dissociation of His92 from the Cu(I) ion is estimated to be 2.4×10^4 s^{-1}. Also, a cooperative effect of the protonation of the remote His61 on the protonation of His92 and the redox properties of the protein was investigated by substituting His61 with asparagine. The mutation causes a modest change in both the pK_a value of His92 and the redox potential of the protein.

Plastocyanin (PCu) is a small blue copper protein of ∼11 kDa (*1*, *2*). It functions as a small mobile electron carrier in the light reactions of photosynthesis in the chloroplast lumen of green plants and green algae, and in the periplasm of many cyanobacteria, where it accepts electrons from cytochrome *f* and transports them to photosystem I. The active redox site of PCu is a copper ion in a distorted tetrahedral conformation ligated to a cysteine (Cys89), two histidines (His39 and His92), and a weakly axially bound methionine (Met97). [Throughout this paper, the amino acid numbers of PCu refer to the sequence of PCu from the cyanobacteria *Anabaena variabilis* (*A.v.*).[1]] The copper binding imidazole group of His92 protrudes through the hydrophobic interface that binds to cytochrome *f* and photosystem I and is thought to facilitate the electron transfer.

In the reduced, native state of most plastocyanins, the His92 residue has a pK_a value of ∼5 (*3*−*7*). Crystallographic studies have shown that upon protonation, the Cu(I) ion changes to a trigonal planar conformation and the His92 imidazole rotates 180° about the C$^\gamma$ −C$^\beta$ bond (*8*). As a result of these structural changes, the redox potential increases, rendering PCu biologically inactive (*9*). Under certain conditions, such as extreme exposure to light, the pH in the thylakoid lumen in plants or the periplasm in bacteria may become highly acidic (pH <6) (*10*). Under these conditions, the protonation of His92 in PCu may be one of the mechanisms that downregulate the photosynthetic activity. This change in plastocyanin is known as the acid transition and has also been observed for several other blue copper proteins such as amicyanin (*11*, *12*), stellacyanins (*4*), mavicyanin (*13*), and pseudoazurin (*14*). In contrast, none of the copper binding histidines in the blue copper proteins azurin (*15*) and rusticyanin (*16*) protonate.

The acid transition has been studied previously by NMR and cyclic voltametry. In the early 1980s, Kojiro and Markley (*17*) concluded on the basis of NMR line-shape studies of *A.v.* PCu that the acid transition is ∼2500 s^{-1} and suggested that the process may involve a rate-determining conformational change. Later, Armstrong et al. (*18*) studied the kinetics using cyclic voltametry but found that the process was too fast to be monitored by this technique. However, they concluded that the transition occurs at a rate faster than 1000 s^{-1} at 3 °C. A more rigorous NMR line-shape study by Lommen and Canters (*12*) showed that the rate is on the order of 10^5 s^{-1} in amicyanin and that the transition is strongly influenced by the presence of buffer. Also, they detected a slower conformational exchange that was observed only for the *protonated* copper site of amicyanin. More recently, it was shown that the acid transition of PCu can be monitored by ^{15}N NMR relaxation measurements through the enhancement of the transverse ^{15}N relaxation rates, R_{ex}, of residues surrounding His92 (*19*), and it was found that the transition takes place between only two forms: a protonated and a deprotonated form. A second protonated conformation like the one observed for amicyanin (*12*) was not detected in *A.v.* PCu. However, as in amicyanin, the acid

† This work was financially supported by Danish Natural Science Research Council Grants 9400351, 9801801, 51-00211, 21-01-0545, and 21-04-0519, Carlsbergfondet Grant 1624/40, Novo Nordisk Fonden Grant 2003-11-28, and Villum Kann Rasmussen Fonden Grant 8.12.2003.

* To whom correspondence should be addressed: Department of Chemistry, University of Copenhagen, Universitetsparken 5, DK-2100 Copenhagen Ø, Denmark. Telephone: (+45) 3532 0302. Fax: (+45) 3535 0609. E-mail: led@kiku.dk.

‡ University of Copenhagen.

§ The Technical University of Denmark.

[1] Abbreviations: *A.v.*, *Anabaena variabilis*; CPMG, Carr−Purcell−Meiboom−Gill; CV, cyclic voltametry; EPG, edge plane graphite; HSQC, heteronuclear single-quantum coherence; NMR, nuclear magnetic resonance; NOESY, nuclear Overhauser effect spectroscopy; TOCSY, total correlation spectroscopy; WT, wild type.

10.1021/bi701446u CCC: $37.00
Published on Web 11/17/2007

transition in PCu was found to be remarkably fast ($\sim 2 \times 10^4$ s^{-1} at pH 5 and 25 °C), considering the fact that the imidazole ring of His92 is ligated to the Cu(I) ion and that only ~7% of the imidazole ring is exposed to the surface according to the crystal structure of PCu (*20*). In fact, the acid transition is too fast to be a direct proton exchange with the solvent water (*19*), because the involved rate constants would exceed the diffusion limit. This indicates that the transition is catalyzed by a buffer that can act as a proton shuttle (*21*). In particular, phosphate is known to enhance proton transfer reactions dramatically (*12*, *21*−*23*).

We have investigated the effect of phosphate buffer on the acid transition to gain further insight into the kinetics and mechanism of the acid transition of plastocyanin in solution. Most importantly, the investigation reveals the presence of a sparsely populated intermediate in the acid transition of *A.v.* PCu. The existence of this intermediate confirms the established view that has emerged from crystallographic studies (*8*), which suggest that the side chain of His92 has to undergo a 180° χ_2 rotation to protonate. Furthermore, investigation enables us for the first time to estimate the rates of the individual steps in the acid transition of plastocyanin.

Also, the pH dependence of the exchange rate can provide information about the mechanism. However, the pH dependence of the exchange rates found previously was difficult to rationalize in terms of a simple two-state mechanism (*19*). Thus, the exchange rate constant was found to decrease with an increase in pH above 6.5, which seems incompatible with the simple acid-base catalysis. Instead, it suggests a negative cooperativity between the protonation of His92 and the protonation of other residues. Such a cooperativity would bias the rate constants, unless it is taken into account. His61 is of particular interest in this context, since it is the only residue in *A.v.* PCu that titrates at neutral pH ($pK_a = 7.06$) where the unexpected pH dependence of the kinetics is observed. It is located ~10 Å from the copper ion, is conserved in most known bacterial plastocyanins, and is present also in plastocyanins from some green algae. For several other blue copper proteins, it has been found that the protonation of histidines on the periphery of the copper site can change the reduction potential significantly, and that this change may be involved in the pH regulation of the copper site reactivity in biological systems (*24*−*26*). His61 in bacterial PCu may have a similar function, and because the effect of the protonation of His61 is likely to be electrostatic, it may influence the pK_a value of His92, giving rise to a cooperative protonation. To further investigate this hypothesis, we have, therefore, mutated His61 to asparagine and examined the effect of the mutation on the protonation of His92 and the reduction potential of the copper site, using NMR spectroscopy and cyclic voltametry.

EXPERIMENTAL PROCEDURES

Preparation of WT and H61N A.v. Plastocyanin. The gene encoding the H61N *A.v.* plastocyanin was obtained by PCR-based site-directed mutagenesis using the QuickChange kit from Stratagene and the WT gene as the template (*19*). The sequence was confirmed by DNA sequencing. WT and H61N uniformly ^{15}N-labeled *A.v.* plastocyanin was expressed and purified as described previously (*20*), except that 4.5 g of $^{15}NH_4Cl$ (in two portions of 0.75 and 3.75 g) was added after depletion of the initial NH_4Cl and before induction of plastocyanin expression. All the NMR samples were prepared as described previously (*19*). The NMR samples contained 1.0 mM ^{15}N-labeled H61N PCu, a 10% D_2O/90% H_2O mixture, and 100 mM NaCl. A small amount of sodium ascorbate was added to the samples to keep the plastocyanins fully reduced.

Five NMR samples of 1.0 mM ^{15}N-labeled reduced WT PCu in a 10% D_2O/90% H_2O mixture were prepared with different sodium phosphate buffer concentrations. The ionic strength of the five samples was adjusted to 0.1 M by adding compensatory amounts of NaCl. The five WT PCu samples contained 0.0, 0.2, 1.0, 10, and 87 mM phosphate buffer. Also, 50 μM sodium ascorbate was added to keep the samples reduced.

NMR Spectroscopy. All NMR experiments were carried out at 298 K. NMR chemical shift titration experiments on ^{15}N-labeled H61N PCu were carried out on a Varian Inova 500 spectrometer operating at a magnetic field strength of 11.7 T, corresponding to a ^{1}H frequency of 499.97 MHz and a ^{15}N frequency of 50.67 MHz. The pH dependence of the ^{15}N chemical shifts of the backbone amide groups was determined from a series of ^{15}N HSQC spectra recorded at 19 different pH values, using a standard gradient-enhanced pulse sequence (*27*). The sweep widths were 10 000 and 2400 Hz in the ^{1}H and ^{15}N dimensions, respectively. The numbers of complex data points acquired in the two dimension were 2048 and 160, respectively. The ^{15}N HSQC spectrum of H61N *A.v.* PCu was assigned using the chemical shift values of WT *A.v.* PCu obtained previously (*19*), and the TOCSY and NOESY spectra of H61N *A.v.* PCu.

NMR relaxation experiments with ^{15}N-labeled H61N and WT PCu were carried out on a Varian Inova 800 spectrometer operating at a magnetic field strength of 18.7 T, corresponding to a ^{1}H frequency of 799.51 MHz and a ^{15}N frequency of 81.02 MHz. All relaxation experiments were conducted within 3 weeks from the time the samples were prepared. Standard HSQC-based R_1 and R_2 experiments, as described by Farrow et al. (*28*), were conducted. Each set of relaxation experiments was recorded on separate samples prepared from the same stock solution. Eight scans were acquired for each FID, using sweep widths of 11 990 and 3400 Hz in the ^{1}H and ^{15}N dimensions, respectively. The numbers of complex data points were 2048 and 180, respectively. Each R_1 experiment consisted of eight spectra with different relaxation delays ranging from 0.01 to 1.9 s, while the R_2 experiments consisted of 11 spectra with relaxation delays ranging from 0.0 to 176 ms. In the ^{15}N R_2 experiments, a CPMG pulse was applied to the protons and the ^{15}N nuclei (*28*). The interpulse delay, τ_{cp}, in the CPMG pulse was 8 ms for ^{1}H and 1 ms for ^{15}N.

Chemical Shift Analysis. The pH dependence of the ^{15}N and ^{1}H chemical shifts of WT PCu was published previously (*19*, *29*). The pH dependence of the ^{15}N and ^{1}H chemical shifts of the backbone amide groups of H61N PCu was analyzed as described previously (*19*). The chemical shift titration curves of H61N PCu were fitted to the observed chemical shifts (see Figure 4), δ_{obs}. For a given nucleus, δ_{obs} is given by

$$\delta_{obs} = \delta_0 + \sum_{i=1}^{N} \frac{\Delta\delta_i}{1 + 10^{pH-pK_{ai}}} \quad (1)$$

where N is the number of titratable residues that affect the chemical shift of the nucleus, $\Delta\delta_i$ is the chemical shift change of the nucleus associated with pK_{ai}, and δ_0 is the chemical shift when all N titrating residues are deprotonated. Equation 1 assumes that all N titrations are mutually independent. The titration curve for each nucleus was fitted independently using eq 1 and increasing values of N until a satisfactory fit was obtained. Subsequently, the $\Delta\delta_i$ contributions were assigned to the protonation of specific groups according to the corresponding pK_{ai} values.

Determination of Exchange Rate Constants, k_{ex}. The exchange rate constant, k_{ex}, for the exchange between protonated and deprotonated His92 was determined from ^{15}N exchange contributions, R_{ex}, derived from the ^{15}N R_2 and R_1 relaxation rates as described previously (*19*, *30*), using the approximation

$$R_{ex} = R_2 - R_1\left\langle\frac{R_2}{R_1}\right\rangle + \Delta_i \quad (2)$$

Here, Δ_i is an empirical correction that compensates for errors introduced by picosecond to nanosecond internal dynamics (*19*, *30*). The Δ_i values determined previously for WT PCu (*19*) were used for H61N PCu. The R_{ex} contributions arising from the protonation−deprotonation process of His92 were analyzed according to a two-site exchange

$$AH^+ \rightleftarrows B + H^+ \quad (3)$$

The exchange rate constant, k_{ex}, was obtained using the equation

$$R_{ex} = \Delta\delta^2\gamma^2 B_0{}^2 p_a p_b \frac{1}{k_{ex}}\left[1 - \frac{2}{\tau_{cp}k_{ex}}\tanh\left(\frac{\tau_{cp}k_{ex}}{2}\right)\right] \quad (4)$$

where

$$p_a p_b = (2 + 10^{pH-pK_a} + 10^{pK_a-pH})^{-1} \quad (5)$$

$\Delta\delta$ is the chemical shift difference between the protonated form, A, and the deprotonated form, B, of His92, while p_a and p_b are the populations of A and B, respectively. Furthermore, B_0 is the magnetic field strength, γ is the gyromagnetic ratio, and τ_{cp} is the interpulse delay of the CPMG pulse train applied to the ^{15}N nuclei in the R_2 experiment. The $\Delta\delta$ and pK_a values were obtained from the chemical shift titration, allowing k_{ex} to be obtained from eq 4. A detailed description of the applied approach was published previously (*19*).

Electrochemistry. Reduction potentials of WT and H61N *A.v.* PCu were measured at different pH values using cyclic voltametry (CV). The pH of the solution was controlled by phosphate buffer prepared by mixing KH_2PO_4 (suprapur, 99.995%, Merck) and K_2HPO_4 (suprapur, 99.99%, Merck). $KClO_4$ (99.99%, Sigma-Aldrich) was used as the supporting electrolyte to increase the ion conductivity.

CV at room temperature (22−23 °C) was performed on an Autolab system (Eco Chemie) controlled by the General Purpose Electrochemical System. The electrochemical cell and electrodes were confined in a Faraday cage to minimize electrical noise. To avoid unnecessary impurities, the reference electrode was a freshly prepared reversible hydrogen electrode, checked against a saturated calomel electrode after each measurement. All potentials reported are versus the normal hydrogen electrode. A clean Pt wire served as the counter electrode. Edge plane graphite (EPG) working electrodes were used. Before each measurement, the EPG was polished with 1.0 and 0.05 μm Al_2O_3 slurry and ultrasonicated twice in Millipore water. The EPG was polished several times for each protein solution, and several cyclic voltamograms at different scan rates were recorded to check both stability and reproducibility. Electrolyte solutions were deoxygenated by Ar (5 N) and purified with Chrompack (<50 ppb oxygen). All glassware was cleaned as previously described (*31*). Millipore (Milli-Q Housing, 18.2 MΩ) water was used throughout.

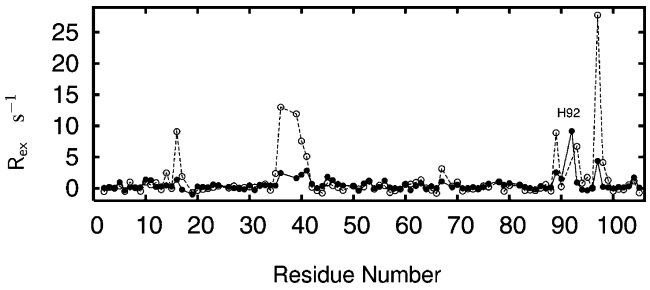

FIGURE 1: R_{ex} contributions in reduced WT *A.v.* PCu at pH 5.3 and 25 °C in the absence of phosphate buffer (○) and in the presence of 87 mM phosphate buffer (●). In the absence of buffer, the signal from His92 was not observed in the relaxation experiments because of extensive line broadening.

RESULTS AND DISCUSSION

Phosphate Catalysis of His92 Protonation. The pH dependence of the exchange rate, k_{ex}, for the protonation of His92 found in previous studies (*19*) of the acid transition of *A.v.* PCu suggests that the rate-determining step in the reaction is the proton transfer step. To further substantiate this suggestion, phosphate buffer was added to freshly prepared samples of WT *A.v.* PCu. Phosphate buffer is known to catalyze proton transfer reactions, and for a simple two-state mechanism, the proton transfer rate increases linearly with buffer concentration (*21*). Therefore, the rate of exchange, k_{ex}, between protonated and deprotonated His92 was measured at four different phosphate concentrations (0.2, 1, 10, and 87 mM) and in the absence of phosphate buffer. The ionic strength was kept constant in all five samples, via addition of compensating amounts of NaCl. No changes in the amide chemical shift upon addition of phosphate were observed, which rules out the formation of a stable complex between His92 and phosphate suggested previously (*12*). Instead, the addition of phosphate caused a dramatic decrease in R_{ex} for the amide ^{15}N nuclei spatially close to the His92 imidazole, as shown in Figure 1 for a 87 mM phosphate buffer at pH 5.3. This decrease in R_{ex} clearly reflects an increase in the exchange rate. Figure 2 shows the exchange rate calculated from the R_{ex} terms, versus the concentration of phosphate buffer. Thus, from the strong dependence of k_{ex} on the phosphate buffer concentration, one can conclude that proton transfer is the rate-limiting step of the His92 protonation at low buffer concentrations. Also, it is worth noticing that even a few hundred micromolar phosphate

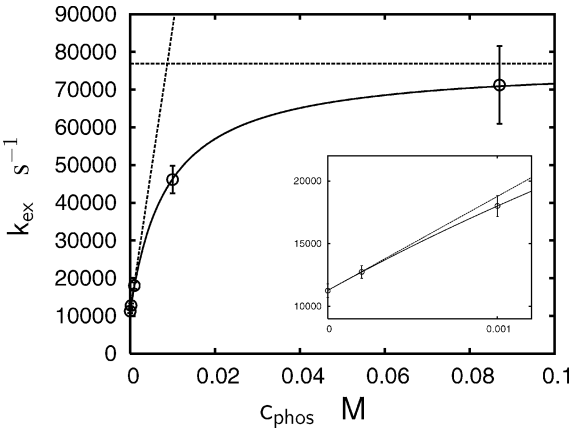

FIGURE 2: Rate of exchange, k_{ex}, between protonated and deprotonated His92 in reduced WT *A.v.* PCu as a function of phosphate buffer concentration at pH 5.3 and 25 °C. The solid line is the least-squares fit of eq 7. The two dashed lines are the extrapolated tangents of the fit at zero and infinite phosphate concentrations. The inset shows a close-up of the data points obtained at low phosphate concentrations.

enhanced the proton transfer significantly, as shown in Figure 2.

Imidazole Rotation. As seen from Figure 2, the dependence of k_{ex} on the phosphate buffer concentration deviates from the linear dependence expected for a two-state mechanism. This nonlinear dependence can be explained if the protonation reaction of His92 includes a sparsely populated intermediate. Crystallographic studies of PCu at different pH values suggest that the protonation of the copper-ligated His92 occurs in at least two steps. First, the imidazole dissociates from the Cu(I) ion and rotates 180°, allowing the N^{δ} atom of the His92 imidazole ring to be exposed to the solvent (*8*). Second, the imidazole ring is protonated. Thus, the protonation reaction of His92 includes at least the following steps

$$B + H_2PO_4^- \underset{k_{-1}}{\overset{k_1}{\rightleftharpoons}} U + H_2PO_4^- \underset{k_2}{\overset{k_{-2}}{\rightleftharpoons}} UH^+ + HPO_4^{2-} \quad (6)$$

where B is the form in which the His92 imidazole ring is bound to the copper ion, U is the form in which it is detached from the copper ion, and UH^+ is the form in which the unbound imidazole ring is protonated. As found experimentally (see above), the proton transfer, i.e., the second step in eq 6, is slow and rate-limiting at low buffer concentrations. However, the rate of the proton transfer increases with an increase in phosphate concentration, making k_{ex} independent of the proton transfer rate at the higher phosphate concentrations. According to eq 6, the exchange rate constant is given by

$$k_{ex} = k_1 \frac{k_{-2}[H_2PO_4^-]}{k_{-1} + k_{-2}[H_2PO_4^-]} + k_2 \frac{k_{-1}[HPO_4^{2-}]}{k_{-1} + k_{-2}[H_2PO_4^-]} + k_0 \quad (7)$$

where k_0 is the exchange rate constant in the absence of phosphate buffer. As shown in Figure 2, eq 7 is in good agreement with the experimental data. According to the analysis using eq 7 (Figure 2), rate constants k_1 and k_2 have values of 2.4×10^4 s^{-1} and 3.9×10^8 s^{-1} M^{-1}, respectively.

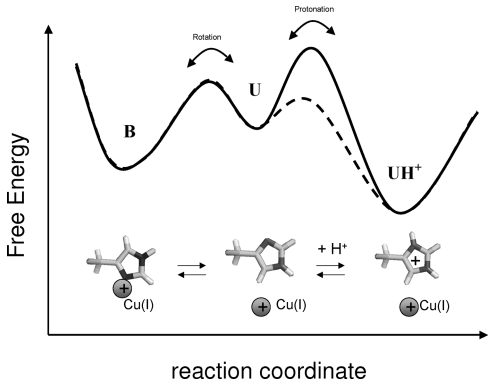

FIGURE 3: Hypothetical mechanism and schematic free energy diagram for the protonation reaction of H92 in plastocyanin at low phosphate concentrations (—) and high phosphate concentrations (– – –).

As suggested above and supported by the crystallographic data, the first step in the proton transfer reaction, eq 6, is the dissociation of the His92 imidazole ring from the Cu(I) ion and a 180° rotation of the ring as sketched in Figure 3. It follows from eq 6 that the observed macroscopic acid dissociation constant is given by

$$K_a = \frac{K_a^U}{K_d} \quad (8)$$

where K_d ($=p_U/p_B$) is the intramolecular dissociation constant for the detachment of His92 from the Cu(I) ion and K_a^U ($= [H^+]p_U/p_{UH^+}$) is the microscopic acid dissociation constant of UH^+. The parameters p_B, p_U, and p_{UH^+} are the populations of the B, U, and UH^+ conformations, respectively.

From eq 7, it can be seen that when $k_{-1} \gg k_{-2}[H_2PO_4^-]$, k_{ex} will depend linearly on the phosphate buffer concentration and protonation is the rate-limiting step. In contrast, when $k_{-1} \ll k_{-2}[H_2PO_4^-]$, k_{ex} is independent of the phosphate concentration and the flipping of the imidazole ring is rate-limiting. In the case where $k_{-1} = k_{-2}[H_2PO_4^-]$, the intermediate is equally likely to become protonated or to flip back and bind the copper ion. The rate constants k_{-1} and k_{-2} cannot be determined independently from the phosphate dependence of k_{ex}. Only their ratio can be determined, which was found to be 8.2 mM. This ratio corresponds to the $H_2PO_4^-$ concentration where both processes are equally fast. However, since the rates of the proton transfers between O- and N-acids and bases of similar strength usually are close to the diffusion limit (*21*), it is possible to give a rough estimate of the population of the intermediate, by assuming a reasonable rate constant at the diffusion limit. For free imidazole, the rate of proton exchange with phosphate is ~4×10^9 s^{-1} M^{-1} (*21*). Here, His92 is partly buried in a hydrophobic protein environment, which most likely will slow the reaction. Therefore, the rate constant was assumed to be between 10^8 and 10^9 s^{-1} M^{-1}. As shown in Table 1, k_{-2} rate constants in this range imply that the intermediate is 0.3−3% populated compared to the copper-bound form of His92. In turn, this implies that the pK_a value of the intermediate is between 6.6 and 7.6, which is a typical range for a surface-exposed histidine not involved in metal binding.

Table 1: Kinetic and Thermodynamic Parameters of the Acid Transition in *A.v.* PCu for Different Values of k_{-2} According to the Reaction Scheme in eq 6[a]

k_{-2} (s^{-1} M^{-1})	K_d	k_{-1} (s^{-1})	k_2 (s^{-1} M^{-1})	k_1 (s^{-1})	pK_a^U
1.0×10^9	3.1×10^{-3}	8.4×10^6	3.9×10^8	2.4×10^4	7.6
5.0×10^8	6.0×10^{-3}	4.1×10^6	3.9×10^8	2.4×10^4	7.3
1.0×10^8	3.0×10^{-2}	8.2×10^5	3.9×10^8	2.4×10^4	6.7

[a] The rate constants k_1, k_2, and k_{-1} were obtained from the fit of eq 7 to the experimental k_{ex} values at different phosphate buffer concentrations. The thermodynamic parameters are derived from the rate constants.

Furthermore, if the $k_{-2} < 10^8$ s^{-1} M^{-1}, a substantial fraction of plastocyanin would be present in the U form (see eq 7), i.e., the intermediate in which His92 is detached from the copper. Since this intermediate, to the best of our knowledge, has never been observed directly by any method, it seems quite unlikely that it should by highly populated. In conclusion, the ranges of kinetic parameters given in Table 1 are consistent with theory and with previous experiments.

Finally, the indication here that proton transfer occurs between the protein and other nonsolvent molecules is in line with intensive studies of the active site protonation of carbonic anhydrase (*32*). Known as one of the most efficient enzymes, carbonic anhydrase requires a very fast proton flux through its active site. This very fast proton flux puzzled researchers for years, because it suggested that the rate of proton transfer reactions exceeded the diffusion limit. The problem was solved when it was realized that buffer molecules are responsible for the proton transfer (*22*, *33*). Thus, the proton is initially transferred to a histidine residue, which subsequently transports the proton to the active site (*32*, *34*).

In the case of plastocyanin and amicyanin, the biological importance of the proton transfer rate as such is unknown. Still, it is interesting that even in the case of histidine protonations, which cannot be related directly to biological function, the rate and mechanism can be similar to the functionally essential protonation of the active site of carbonic anhydrase. Moreover, these considerations suggest that under physiological conditions, direct proton transfer from solvent water to histidine residues is of little importance, because the physiological concentration of buffer molecules is several orders of magnitude larger than the OH^- and H^+ concentrations. Another striking aspect of the His92 protonation is that it requires a fast rotation of the imidazole group, i.e., 2.4×10^4 s^{-1} or faster. This may seem counterintuitive since His92 is ligating the copper ion and several side chains pack closely against the imidazole ring. Thus, the fast rotation suggests a substantial flexibility of the copper site and its proximity. The rotation is probably facilitated by even faster overall motions on the nanosecond or even picosecond time scale, which open up the structure sufficiently to accommodate the imidazole rotation. Therefore, the rotation of the imidazole may be an indicator of the copper site dynamics, a characteristic that may be important for the unique redox properties of blue copper proteins.

Protonation Rate in the Absence of Buffer. Above, the kinetics of the acid transition was studied through the buffer dependence of the exchange rate, k_{ex}. Below, the pH dependence of k_{ex} is investigated in the absence of added buffers, to establish consistency with previous studies of the pH dependency of the kinetics carried out in unbuffered solutions (*19*). These studies showed several unexpected results. Thus, in the absence of buffer molecules, the proton transfer should in principle be a purely specific, acid-base-catalyzed transfer. However, this model is inconsistent with the previous results. To clarify this inconsistency, we here investigate two possible effects: (i) an interference from an anticooperative protonation between His92 and the remote His61 and (ii) a general acid-base catalysis by one or more unidentified buffers. As shown below, these two effects together can explain the previously observed pH dependence of the protonation of His92 in the absence of added buffer. The former effect is studied by comparing WT *A.v.* PCu with its H61N mutant through differences in chemical shifts, pK_a values, and redox potentials, while the latter effect is studied by analyzing the pH dependence of k_{ex} of both WT and H61N PCu. To evaluate the effect of the deprotonation of His61 on the structure of the Cu(I) site of PCu, and to investigate a possible cooperativity between the protonation and deprotonation of His61 and the copper ligand His92, His61 was mutated to asparagine. Asparagine was chosen because it has no net charge.

Chemical Shift Analysis of H61N PCu. H61N *A.v.* PCu contains 13 groups that titrate in the pH range from 3 to 9. The pH dependence of all the observed chemical shifts could be fitted satisfactorily by eq 1, including from zero to two titrations. The titratable groups in H61N *A.v.* PCu include five glutamate and five aspartate side chains, the C-teminal carboxylate group, the N-terminal amino group, and His92. The titration of His92 is clearly the titration that affects the most nuclei, whereas the $\Delta\delta_i$ values caused by other titrations are comparably smaller on an average. Carboxylate groups in WT and H61N PCu have pK_a values below 5, with the exception of Glu30, which has a pK_a value similar to that of His92 (*19*). However, the impact from Glu30 titration is considerably smaller than the effect from His92. Therefore, titrations associated with pK_{ai} values from 5.2 to 5.6 were assigned to His92 except for residues within 9 Å of the carboxylate group of Glu30. From the average of the pK_{ai} values assigned to the His92 titration for individual nuclei, a pK_a value of 5.41 ± 0.01 was obtained for His92 in H61N PCu. Titrations associated with a pK_{ai} of <5.2 were assigned to carboxylate groups, and titrations with a pK_{ai} of >7 were assigned to the N-terminal amino group.

Comparison of WT and H61N PCu NMR Chemical Shifts. A possible change in the structure of the Cu(I) site of PCu induced by the H61N mutation was investigated by comparing the amide chemical shifts of H61N PCu and the His6-deprotonated form of WT PCu at pH 7.0. The chemical shifts of His61-deprotonated WT PCu were calculated from the parameters previously obtained from the chemical shift titration curves of WT PCu (*19*, *29*). It was found that the differences in chemical shift are modest, ranging from -2.3 to 1.5 ppm for the amide ^{15}N and from -0.32 to 0.37 ppm for the amide protons, the average values being 0.23 ppm for ^{15}N and 0.052 ppm for protons as shown in Figure 5. The largest changes are observed for residues S60−L64, H39−V41, and S71−T75. These three regions are in the immediate proximity of the His61 imidazole ring in WT PCu where chemical shift changes are expected because of the removal of the aromatic ring. [It should be noted that in the crystal structure of *A.v.* PCu (*20*), the side chain of His61

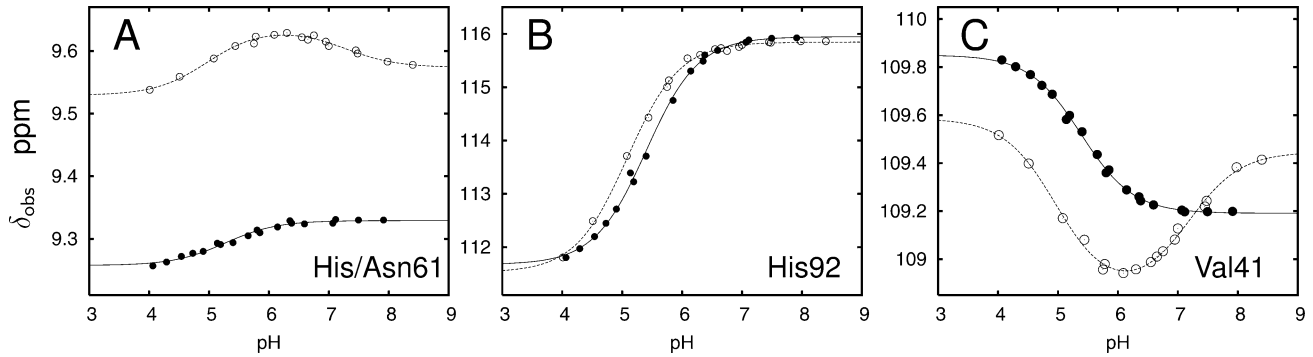

FIGURE 4: Backbone amide ^{15}N and ^{1}H chemical shift titration data at 25 °C of reduced WT *A.v.* PCu (○) and H61N *A.v.* PCu (●) for three different nuclei: (A) amide ^{1}H of residue 61, (B) amide ^{15}N of His92, and (C) amide ^{15}N of Val41. The dashed and solid lines represent the least-squares fit of eq 1 to the chemical shifts of WT and H61N PCu, respectively.

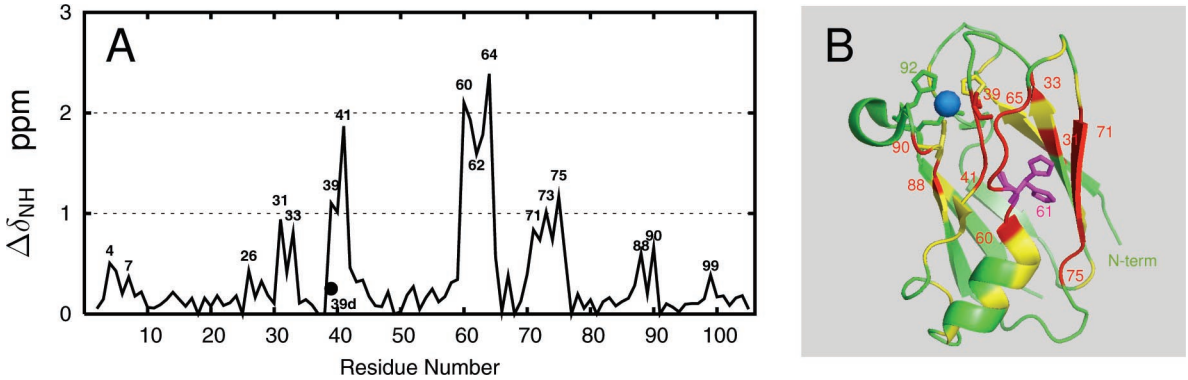

FIGURE 5: Difference in the amide chemical shift, $\Delta\delta_{NH}$, between H61N *A.v.* PCu and WT *A.v.* PCu where His61 is deprotonated. Panel A shows the combined amide proton and nitrogen chemical shift difference, $\Delta\delta_{NH} = \sqrt{(\Delta\delta_N)^2 + (5\Delta\delta_H)^2}$. The black dot (●) represents the value of the NH group of the copper-ligated imidazole ring of His39. In panel B, the structure of WT *A.v.* PCu (PDB entry 2GIM) (*20*) is colored according to the size of $\Delta\delta_{NH}$: red for $\Delta\delta_{NH} \geq 0.5$ ppm, yellow for 0.5 ppm > $\Delta\delta_{NH}$ > 0.2 ppm, and green for $\Delta\delta_{NH} \leq 0.2$ ppm. His61 with its two side chain conformations is colored magenta, and the copper ion is colored blue.

assumes two different rotamers, one in which the imidazole ring is oriented toward residues K62−L64 and H39−V41 and one in which the imidazole ring interacts with residues T72−T74.] Smaller chemical shift differences are also observed in regions more distant from the position of residue 61, such as G26−N33, T4−L7, Y88, E90, and G99. These differences may be caused by subtle structural changes in the structure.

Most importantly, the chemical shifts of the C-terminal copper binding loop, residues C89−M97, are affected very little by the mutation, and only the copper ligand, His39, shows a sizable change in the backbone chemical shift while the N$^{\epsilon}$ and H$^{\epsilon}$ atoms of its copper binding imidazole group have unchanged chemical shifts. Therefore, the NMR data suggest that the H61N mutant closely mimics the His61-deprotonated form of WT PCu with respect to the structure of the copper site and the structure around His92. This conclusion is further supported by the chemical shifts changes, $\Delta\delta$, observed for the amide ^{15}N and ^{1}H nuclei in the WT and H61N plastocyanins upon protonation of His92 (see eq 1). Thus, the $\Delta\delta$ values are almost unchanged for all corresponding residues, including all four copper ligands, in the two plastocyanins.

Anticooperative Protonations of His92 and His61. From the pH dependence of the amide ^{1}H and ^{15}N chemical shifts, the pK_a of His92 in H61N *A.v.* PCu was found to be 5.41 ± 0.01, which is 0.32 pH unit larger than the pK_a of 5.09 ± 0.01 obtained for His92 in WT *A.v.* PCu (*19*). Examples of the chemical shift titrations are shown in Figure 4. It is unlikely that structural changes are the reason for the larger pK_a of H61N PCu, since the mutation seems to have little effect on the structure of the His92 environment, as discussed above. More likely, the increase in the pK_a is caused by an electrostatic effect. Thus, in WT PCu, the His61 residue is protonated and carries a positive charge when His92 titrates. In contrast, in the H61N mutant, this charge is absent and the pK_a of His92 is increased by 0.32 pH unit, corresponding to a 1.8 kJ/mol stabilization of the protonated form of His92. This value is close to the values of the electrostatic interaction free energy obtained using finite-size dielectric continuum models for the globular protein embedded in a dielectric solvent environment (*35*, *36*). Therefore, the results here indicate an anticooperative effect between the protonations of His92 and His61, whereby the deprotonation of His61 stabilizes the protonated form of His92 by 1.8 kJ/mol.

Changes in the Redox Potential of PCu. Electrostatic effects responsible for the change in the pK_a value of His92 are likely also to affect the redox properties of the copper ion, since the imidazole ring of His92 and the copper ion are very close to each other. Therefore, the reduction potential of both WT and H61N *A.v.* PCu was measured at different pH values.

Previous studies of PCu from *A. variabilis* and *Scenedesmus obliquus* (*37*, *38*) indicated an electrostatic interaction between the copper ion and a charge at position 61. Both of

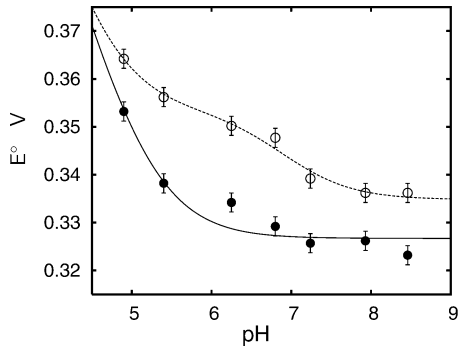

FIGURE 6: Reduction potential of WT *A.v.* PCu (○) and H61N *A.v.* PCu (●) vs pH at room temperature. The solid and dotted lines represent the least-squares fit of a single and double titration to the reduction potential of H61N and WT PCu, respectively.

these plastocyanins have a His in position 61, and for both of them, a pH-dependent redox potential was observed, the reduction potentials being increased by ~15 mV when the pH is decreased over a pH range around pH 7 where H61 titrates. With a further decrease in pH, a larger increase in the reduction potential is observed due to the His92 protonation.

The pH dependence of the reduction potential of WT *A.v.* PCu was analyzed using

$$E^\circ = E_0 + \frac{RT}{nF}\left[\ln(1 + 10^{pK_a - pH}) + \ln\left(\frac{1 + 10^{pK_a^{red} - pH}}{1 + 10^{pK_a^{ox} - pH}}\right)\right] \quad (9)$$

where pK_a is the acid dissociation constant of His92 in reduced PCu and pK_a^{red} and pK_a^{ox} are the acid dissociation constants of His61 in reduced and oxidized PCu, respectively. Furthermore, R is the molar gas constant, F is the Faraday constant, n is the number of electrons, T is the absolute temperature, and E_0 is the reduction potential of PCu where both His92 and His61 are deprotonated.

The analysis of the pH dependence of the reduction potential of WT *A.v.* PCu obtained here supports the electrostatic interaction between His61 and His92. Thus, an analysis of the data in Figure 6 using eq 9 gave pK_a values of 7.0 ± 0.2 and 6.7 ± 0.2 for His61 in the reduced and the oxidized form of WT *A.v.* PCu, respectively, while the difference between the two pK_a values is 0.3 ± 0.05. Notice that the difference is more accurately determined than the pK_a values themselves, because the errors in the pK_a values are correlated. For the pK_a of His92 in the reduced form of *A.v.* PCu, a value of 4.6 ± 0.2 was obtained, in reasonable agreement with the value of 5.1 obtained by NMR (*19*). Qualitatively, the increase in the His61 pK_a value upon reduction of PCu shows that His61 is more easily protonated, and thus more easily charged, if the copper ion is only singly charged, as Cu^+ in the reduced form, than if the copper ion is doubly charged, as Cu^{2+} in the oxidized form. Quantitatively, the difference of 0.3 pH unit between the His61 pK_a value of reduced and oxidized PCu corresponds to a 1.7 kJ/mol stabilization of oxidized PCu when His61 is deprotonated, in good agreement with the 1.8 kJ/mol stabilization of the His92-protonated form of reduced PCu when position 61 is uncharged, as indicated by the comparison of WT and H61N PCu (see above).

The pH dependence of the reduction potential of H61N *A.v.* PCu was also analyzed. Using eq 9 while omitting the second logarithmic term and assuming a single titration model, the analysis resulted in a pK_a value of 5.1 ± 0.1 for His92 in reduced H61N PCu. At pH >8, the reduction potential of the mutant is ~10 mV smaller than that of WT PCu, as shown in Figure 6. This difference is likely to reflect effects other than electrostatic effects, e.g., structural. A residual bimodal feature in the E°/pH profile of the mutant protein can in fact be distinguished in Figure 6. However, using the full eq 9, the amplitude of the pH 6−9 region is only 8−10 mV, i.e., significantly smaller than for the WT protein and close to the E° difference between the two proteins at the high-pH limit. This seems to indicate also that minor structural effects are induced by the H61N mutation, in addition to the purely electrostatic effects.

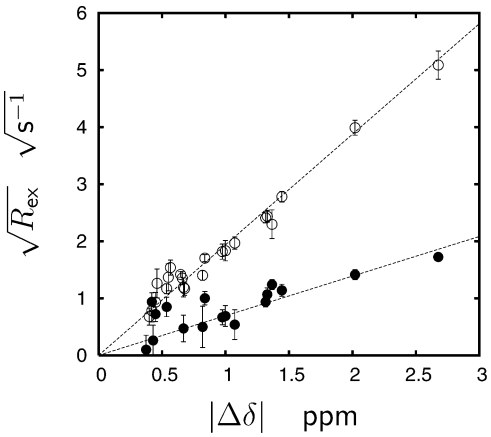

FIGURE 7: Square root of R_{ex} vs the change in the ^{15}N chemical shift, $|\Delta\delta|$, associated with His92 protonation in reduced H61N *A.v.* PCu at pH 6.86 (●) and pH 5.88 (○). The lines represent least-squares linear fits to the equation $\sqrt{R_{ex}} = f(|\Delta\delta|)$ according to eq 4.

Thus, overall, the electrochemical studies of the WT protein support the NMR results, and together, the two approaches support the suggestion of anticooperative protonation of His92 and His61 caused by a primarily electrostatic interaction of ~1.8 kJ/mol between the two residues in WT PCu.

Exchange Rate in H61N A.v. PCu of the Protonation and Deprotonation of His92. The rate of exchange, k_{ex}, between the His92-protonated and deprotonated form was obtained from the ^{15}N exchange contributions, R_{ex}, as described previously (*19*). The k_{ex} rates were determined from the slope of $\sqrt{R_{ex}}$ as a function of $|\Delta\delta|$, according to eq 4 (see Figure 7). The obtained exchange rates, k_{ex}, show a decreasing trend with an increase in pH below pH 6 and an increasing trend above pH 6. Thus, a decreasing trend around pH 7 is not observed in contrast to previous studies of the WT protein (*19*). Except for this difference, the rate constants are very similar to those previously obtained for WT PCu.

Importance of the Anticooperative Protonation for the Determination of k_{ex} in WT PCu. As discussed above, the elevated pK_a value of His92 in H61N suggests that the pK_a of His92 in WT PCu increases upon deprotonation of His61. Electrochemical measurements support this suggestion. In principle, this anticooperative protonation also influences the chemical shift titration curves of WT PCu. However, because of the small change in the pK_a of His92 caused by the anticooperativity and because of the large difference in the pK_a values of His61 and His92, the effect will be too small

to be observed, yet the anticooperativity has a significant effect on the exchange contributions caused by His92 protonation at neutral pH. At pH 7, there is only ~1% of the protonated form of His92, and the exchange contribution is proportional to this population, according to eq 4. A change in the pK_a of His92 by 0.3 pH unit upon full protonation of His61 will double the population of the protonated form of His92 and, thereby, double the exchange contribution. Consequently, the exchange rate constant, k_{ex}, that can be derived from R_{ex} using eqs 4 and 5 will be underestimated by a factor of up to 2 when His61 is fully protonated, since the exchange contribution depends approximately inversely on the exchange rate.

The effect of anticooperativity between the protonations of His92 and His61 on the exchange rate constant, k_{ex}, can be included in the calculation of k_{ex} by introducing a pH-dependent pK_a value of His92:

$$pK_a = pK_{a0} + \frac{\Delta pK_a}{1 + 10^{pK_{a1} - pH}} \qquad (10)$$

where pK_{a0} is the pK_a of His92 at low pH obtained from the chemical shift titration curves, pK_{a1} is the pK_a of His61, and ΔpK_a is the increase in the pK_a of His92 when His61 deprotonates. In the previous study of the pH dependence of the k_{ex} exchange rate for WT PCu (*19*), we observed an apparent decreasing trend in k_{ex} with an increase in pH above 7, which is not observed in H61N PCu. However, if the pH dependence of the pK_a of His92 can be taken into account using eq 10, the apparent decreasing trend in k_{ex} can be eliminated. This is shown in Figure 8A, where, by and large, the decreasing trend is eliminated for a ΔpK_a of 0.3. Therefore, the trend previously observed for WT PCu can be interpreted as an artifact, which arises if the anticooperativity between His61 and His92 protonation is neglected. In the following, the exchange rate constants of WT PCu are corrected for anticooperativity using eq 10 and a ΔpK_a of 0.3.

Kinetic Model for the His92 Proton Transfer. The pH dependence of k_{ex} contains information about the mechanism of the proton exchange of His92. The simplest mechanism involves a proton transfer from the solvent water, i.e., a specific acid-base catalysis. If both protonation by protons and deprotonation by hydroxide ions are included, k_{ex} is given by

$$k_{ex} = k_2^{OH} K_w([H^+]^{-1} + K_a^{-1}) + k_2^{H}([H^+] + K_a) \qquad (11)$$

However, as shown in Figure 8B, this model provides only a poor fit to the experimental data. Moreover, the obtained rate constants, k_2^{OH} and k_2^{H}, are $\sim 2 \times 10^{11}$ and 1.5×10^9 M^{-1} s^{-1}, respectively, for both WT and H61N PCu; that is, the obtained second-order rate constant for the OH^- catalysis exceeds the fast diffusion limit of 10^{11} M^{-1} s^{-1}. By way of comparison, k_2^{OH} and k_2^{H} of free imidazole in dilute aqueous solutions are both $\sim 2 \times 10^{10}$ M^{-1} s^{-1} at 25 °C (*21*). In the case of His92 protonation, one would expect a rate constant well below this value, because the protonation of the imidazole ring of His92 is competing with the copper binding. Therefore, the proton transfer of His92 in PCu cannot occur directly between His92 and the solvent water. Instead, the proton transfer must be catalyzed by other components that mediate the proton transfer, such as buffers and impurities in the NMR samples, or other acidic and basic groups within the plastocyanin molecule itself, all of which may act as general acid-base catalysts. Here, an intramolecular proton transfer seems unlikely since the imidazole ring is surrounded by hydrophobic residues, and no acidic or basic groups are close to the imidazole group. Instead, an intermolecular proton transfer seems probable. Even though no buffer was added to the NMR samples, impurities in the sample or remnants of buffer used during the purification may be present.

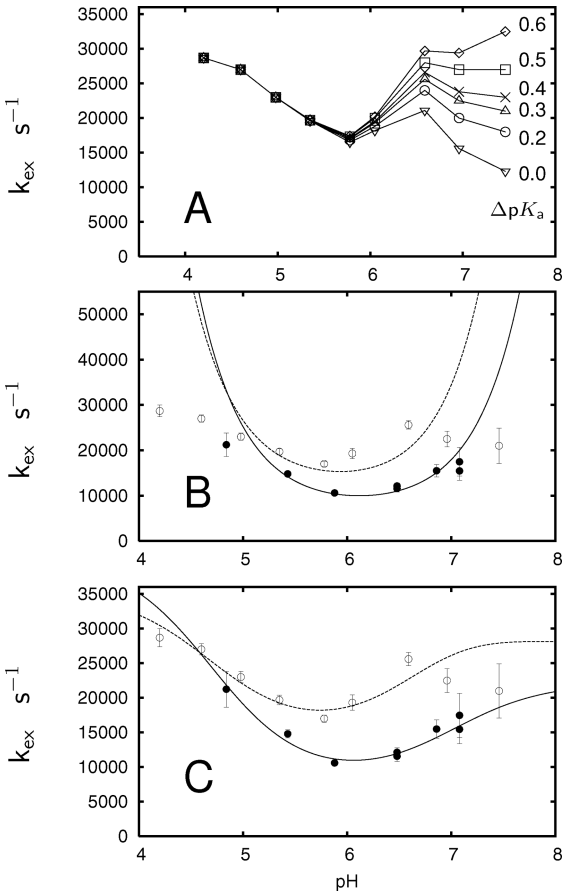

FIGURE 8: Rate of exchange, k_{ex}, of protonation/deprotonation of His92 vs pH in reduced WT *A.v.* PCu (○) and H61N *A.v.* PCu (●) at 25 °C. The exchange rates were calculated from the experimental relaxation data. Panel A shows the effect of the anticooperative protonation of His92 and His61 on the exchange rate obtained for WT *A.v.* PCu for a series of values of ΔpK_a, the increase of pK_a of WT PCu caused by the anticooperativity (see eq 10). In panels B and C, the exchange rates of WT PCu were calculated assuming a cooperativity of ΔpK_a = 0.3. In panel B, the exchange rates are analyzed according to the specific acid-base mechanism (eq 11). In panel C, the exchange rates are analyzed according to the general acid-base catalysis with two catalytic species with different pK_a values (see the text).

Although the precise amount of impurities in the NMR samples here is not known, it is likely that the total amount of acidic and basic impurities is in the range of 0.1−1 mM, even in the most carefully prepared samples. Also, since the native protein itself is a buffer, protons may exchange between the plastocyanin molecules. Transient self-association has previously been observed for *A.v.* PCu by paramagnetic NMR (*39*). Thus, the protein concentration is 1 mM, and the protein molecule has 24 titratable groups at the surface of the molecule, that is, 12 side chain carboxylate

groups, two histidine imidazole side chains, nine side chain amino groups, and one arginine. Therefore, the native protein itself may contribute substantially to the exchange rate. Unfortunately, it is difficult experimentally to distinguish this contribution from those caused by impurities, since a dilution of the protein concentration also dilutes the concentration of the impurities. Finally, as found previously (*30*), samples that were only a few weeks old exhibited significantly smaller R_{ex} values than freshly prepared samples, indicating an enhanced exchange rate. The chemical shift values in these samples remained unchanged compared to those of freshly prepared samples; however, weak signals from a small amount of denatured protein were clearly visible in the HSQC spectra of the older samples. Thus, a buildup of acidic and basic impurities produced by minor denaturation followed by slow peptide hydrolysis could plausibly give rise to the enhanced exchange rates observed in older samples.

The general acid-base catalysis is described by

$$B + X^iH^+ \underset{k_{2\text{-}i}}{\overset{k_{2i}}{\rightleftharpoons}} UH^+ + X^i \qquad (12)$$

where X^iH^+ and X^i are the general acid-base catalysts, respectively. Here the intermediate, U (see eq 6), is ignored because the rearrangement is far from being rate-limiting when no buffer is added to the samples, and therefore, the presence of this sparsely populated intermediate does not affect the pH dependence of k_{ex}. From eq 12, it follows that the exchange rate constant, k_{ex}, for the general acid-base-catalyzed, intermolecular proton exchange is given by

$$k_{ex} = \sum_{i=1}^{N} c_i k_{2i} \left[\left(1 + \frac{K_i}{[H^+]} \right)^{-1} + \frac{K_a}{K_i} \left(1 + \frac{[H^+]}{K_i} \right)^{-1} \right] \qquad (13)$$

where c_i, k_{2i}, and K_i are the total concentrations, the second-order rate constants, and the acid dissociation constants of the acid catalysts, X^iH^+, respectively. N is the total number of different catalytic acid-base pairs. The simplest model, which can account for the observed pH dependence of k_{ex}, involves two species ($N = 2$). It should be noted that the actual pK_a values of the catalytic species cannot be derived, since basically any combination of pK_a values gives satisfactory fits to the experimental data. Only it is required that at least one of the pK_i values be larger and one smaller than the pK_a of His92. Thus, the pK_a values were set to pK_1 = 4.7 and pK_2 = 7.0 in the fit shown in Figure 8C, while the concentration (c_i) was 1 mM. For these parameters, rate constants of 4×10^7 M^{-1} s^{-1} (k_{21}) and 4×10^5 M^{-1} s^{-1} (k_{22}) were obtained for H61N PCu, while rates constants of 3×10^7 and 5×10^5 M^{-1} s^{-1} were obtained for WT PCu. The second-order rate constants thus obtained can only be interpreted qualitatively; the orders of magnitude are still reasonable. It is, therefore, concluded that the fast proton exchange of His92 takes place according to the general acid-base mechanism also in samples where no buffer has been added.

CONCLUSIONS

In conclusion, the study provides new insight into the mechanism of the acid transition of plastocyanin. It is shown that the acid transition in *A.v.* plastocyanin is a two-step process, which at low buffer concentrations is rate-limited by proton transfer between His92 and the buffer. At high buffer concentrations, the other step becomes rate-limiting. This step is most likely a step in which the imidazole ring of His92 detaches from the copper and rotates 180°. Thus, via measurement of the rate of the acid transition at high buffer concentrations, the rate of dissociation and rotation of the copper binding imidazole ring of His92 is obtained. In turn, this rate may provide a way to probe the intrinsic dynamics of the copper site in plastocyanins as well as in other blue copper proteins.

Also, it shows that the proton transfer does not take place directly between the copper-ligated His92 and solvent water, according to a specific acid-base catalysis. Instead, the proton transfer step in the acid transition is governed by general acid-base catalysis under all the sample conditions applied here. Thus, like in other enzyme-catalyzed protonations (*32*, *34*), the protonation/deprotonation involves a buffer, which accelerates the process dramatically. The extreme sensitivity of the proton exchange rate, k_{ex}, with respect to even small concentrations of acidic and basic molecules is illustrated by adding increasing amounts of phosphate buffer to the sample. In the absence of added buffer, the proton transfer is still active. Although we cannot decide which molecules catalyze the process under these circumstances, it is likely that small amounts of impurities arising from the protein purification or degradation of the protein, or ascorbate added to avoid oxidation, may catalyze the proton transfer. In addition, proton transfer may also occur between different protein molecules with many acidic and basic groups on their surface such as the plastocyanin molecule, even at concentrations of 1 mM.

Elucidation of the pH dependence of the proton transfer mechanism obtained here relies partly on the determination of an anticooperativity between the protonations of His92 and His61. Thus, the studies here of the H61N mutant of *A.v.* PCu reveal an electrostatic interaction (1.8 kJ/mol) between His92 and His61 located 13−15 Å from each other, which gives rise to the anticooperativity. When the anticooperativity is included in the derivation of k_{ex} from the ^{15}N relaxation data, the pH profile of the kinetics is in agreement with a general acid-base catalysis.

ACKNOWLEDGMENT

We thank Jens Ulstrup, Malene R. Jensen, D. Flemming Hansen, and Søren M. Kristensen for helpful discussions and Lise-Lotte Jespersen, Jens Ø. Duus, and Bent O. Petersen for technical assistance. The 800 MHz spectra were acquired at The Danish Instrument Center for NMR Spectroscopy of Biological Macromolecules.

SUPPORTING INFORMATION AVAILABLE

Tables of the ^{15}N and ^1H chemical shifts of all nuclei that can be observed in the ^{15}N HSQC spectrum of H61N *A.v.* PCu. This material is available free of charge via the Internet at http://pubs.acs.org.

REFERENCES

1. Hope, A. B. (2000) Electron transfer amongst cytochrome *f*, plastocyanin and photosystem I: Kinetics and mechanisms, *Biochim. Biophys. Acta 1456*, 5−26.

2. Sigfridsson, K. (1998) Plastocyanin, an electron-transfer protein, *Photosynth. Res. 57*, 1−28.
3. Markley, J. L., Ulrich, E. L., Berg, S. P., and Krogmann, D. W. (1975) Nuclear Magnetic Resonance Studies of Copper Binding Sites of Blue Copper Proteins: Oxidized, Reduced, and Apoplastocyanin, *Biochemistry 14*, 4428−4433.
4. Battistuzzi, G., Borsari, M., Canters, G. W., de Waal, E., Leonardi, A., Ranieri, A., and Sola, M. (2002) Thermodynamics of the Acid Transition in Blue Copper Proteins, *Biochemistry 41*, 14293−14298.
5. Dennison, C., Lawler, A. T., and Kohzuma, T. (2002) Unusual Properties of Plastocyanin from the Fern *Dryopteris crassirhizoma*, *Biochemistry 41*, 552−560.
6. Hunter, D. M., McFarlane, W., Sykes, A. G., and Dennison, C. (2001) Effect of pH on the Self-Exchange Reactivity of the Plant Plastocyanin from Parsley, *Inorg. Chem. 40*, 354−360.
7. Hulsker, R., Mery, A., Thomassen, E. A., Ranieri, A., Sola, M., Verbeet, M. P., Kohzuma, T., and Ubbink, M. (2007) Protonation of a histidine copper ligand in fern plastocyanin, *J. Am. Chem. Soc. 129*, 4423−4429.
8. Guss, J. M., Harrowell, P. R., Murata, M., Norris, V. A., and Freeman, H. C. (1986) Crystal structure analyses of reduced (Cu^{I}) poplar plastocyanin at six pH values, *J. Mol. Biol. 192*, 361−387.
9. Canters, G. W., Kolczak, U., Armstrong, F., Jeuken, L. J. C., Camba, R., and Sola, M. (2000) The effect of pH and ligand exchange on the redox properties of blue copper proteins, *Faraday Discuss. 116*, 205−220.
10. Kramer, D. M., Sacksteder, C. A., and Cruz, J. A. (1999) How acidic is the lumen? *Photosynth. Res. 60*, 151−163.
11. Lommen, A., Canters, G. W., and van Beeumen, J. (1988) A ^{1}H-NMR Study on the Blue Copper Protein Amicyanin from *Thiobacillus versutus*. Resonance Identifications, Structural Rearrangements and Determination of the Electron Self-Exchange Rate Constant, *Eur. J. Biochem. 176*, 213−223.
12. Lommen, A., and Canters, G. W. (1990) pH-dependent Redox Activity and Fluxionality of the Copper Site in Amicyanin from *Thiobacillus yersutus* as Studied by 300- and 600-MHz ^{1}H NMR, *J. Biol. Chem. 265*, 2768−2774.
13. Battistuzzi, G., Borsari, M., Loschi, L., Ranieri, A., Sola, M., and B. Mondovì, A. M. (2001) Redox properties and acid−base equilibria of zucchini mavicyanin, *J. Inorg. Biochem. 83*, 223−227.
14. Dennison, C., Kohzuma, T., McFarlane, W., Suzuki, S., and Sykes, A. G. (1994) Reactivity of Pseudoazurin from *Achromobacter cycloclastes* with Inorganic Redox Partners and Related NMR and Electrochemical Studies, *Inorg. Chem. 33*, 3299−3305.
15. Jeuken, L. J. C., van Vliet, P., Verbeet, M. P., Camba, R., McEvoy, J. P., Armstrong, F. A., and Canters, G. W. (2000) Role of the Surface-Exposed and Copper-Coordinating Histidine in Blue Copper Proteins: The Electron-Transfer and Redox-Coupled Ligand Binding Properties of His117Gly Azurin, *J. Am. Chem. Soc. 122*, 12186−12194.
16. Butuyan, M. V., Toy-Palmer, A., Chung, J., Blake, R. C., II, Beroza, P., Case, D. A., and Dyson, H. J. (1996) NMR Solution Sturucture of Cu(I) Rusticyanin from *Thiobacillus ferrooxidans*: Structural Basis for the Extreme Acid Stability and Redox Potential, *J. Mol. Biol. 263*, 752−767.
17. Kojiro, C. L., and Markley, J. L. (1983) Connectivity of proton and carbon spectra of the blue copper protein, plastocyanin, established by two-dimensional nuclear magnetic resonance, *FEBS Lett. 162*, 52−56.
18. Armstrong, F. A., Hill, H. A. O., Oliver, B. N., and Whitford, D. (1985) Direct Electrochemistry of the Photosynthetic Blue Copper Protein Plastocyanin. Electrostatic promotion of Rapid Charge Transfer at the Edge-Oriented Pyrolytic Graphite Electrode, *J. Am. Chem. Soc. 107*, 1473−1476.
19. Hass, M. A. S., Thuesen, M. H., Christensen, H. E. M., and Led, J. J. (2004) Characterization of μs-ms Dynamics of Proteins Using a Combined Analysis of ^{15}N NMR Relaxation and Chemical Shift: Conformational Exchange in Plastocyanin Induced by Histidine Protonations, *J. Am. Chem. Soc. 126*, 753−765.
20. Schmidt, L., Christensen, H. E. M., and Harris, P. (2006) 1.6 Å structure of plastocyanin from *Anabaena variabilis*, *Acta Crystallogr. D62*, 1022−1029.
21. Eigen, M. (1963) Protonenübertragung, Säure-Base-Katalyse und enzymatische Hydrolyse. Teil I: Elementarvorgänge, *Angew. Chem. 75*, 489−508.
22. Khalifah, R. G. (1973) Carbon Dioxide Hydration Activity of Carbonic Anhydrase: Paradoxical Consequences of the Unusully Rapid Catalysis, *Proc. Natl. Acad. Sci. U.S.A. 70*, 1986−1989.
23. Sudmeier, J. L., Evelhoch, J. L., and Jonsson, N. B.-H. (1980) Dependence of NMR Lineshape Analysis upon Chemical Rates and Mechanisms: Implications for Enzyme Histidine Titrations, *J. Magn. Reson. 40*, 377−390.
24. Kalverda, A. P., Ubbink, M., Gilardi, G., Wijmenga, S. S., Crawford, A., Jeuken, L. J. C., and Canters, G. W. (1999) Backbone Dynamics of Azurin in Solution: Slow Conformational Change Associated with Deprotonation of Histidine 35, *Biochemistry 38*, 12690−12697.
25. Dennison, C., and Lawler, A. T. (2001) Investigation of the Alkaline and Acid Transition of Umecyanin, a Stellacyanin from Horseradish Roots, *Biochemistry 40*, 3158−3166.
26. Sato, K., and Dennison, C. (2002) Effect of Histidine 6 Protonation on the Active Site Structure And Electron-Transfer Capabilities of Pseudoazurin from *Achromobacter cycloclastes*, *Biochemistry 41*, 120−130.
27. Zhang, O., Kay, L. E., Olivier, J. P., and Forman-Kay, J. D. (1994) Backbone ^{1}H and ^{15}N resonance assignments of the N-terminal SH3 domain of drk in folded and unfolded states using enhanced-sensitivity pulsed field gradient NMR techniques, *J. Biomol. NMR 4*, 845−858.
28. Farrow, N. A., Muhandiram, R., Singer, A. U., Pascal, S. M., Kay, C. M., Gish, G., Shoelson, S. E., Pawson, T., Forman-Kay, J. D., and Kay, L. E. (1994) Backbone Dynamics of Free and a Phosphopeptide-Complexed Src Homology 2 Domain Studied by ^{15}N NMR Relaxation, *Biochemistry 33*, 5984−6003.
29. Hass, M. A. S., Jensen, M. R., and Led, J. J. (2007) Probing Electric Fields in Proteins in Solution by NMR (submitted for publication).
30. Hass, M. A. S., and Led, J. J. (2006) Evaluation of two simplified N-15-NMR methods for determining μs-ms dynamicsm of proteins, *Magn. Reson. Chem. 44*, 761−769.
31. Zhang, J., Chi, Q., Nielsen, J. U., Friis, E. P., Andersen, J. E. T., and Ulstrup, J. (2000) Two-dimensional cysteine and cystine cluster networks on Au(111) disclosed by voltametry and in situ scanning tunneling microscopy, *Langmuir 16*, 7229−7237.
32. Lindskog, S. (1997) Structure and Mechanism of Carbonic Anhydrase, *Pharmacol. Ther. 74*, 1−20.
33. Lindskog, S., and Coleman, J. E. (1973) The Catalytic Mechanism of Carbonic Anhydrase, *Proc. Natl. Acad. Sci. U.S.A. 70*, 2505−2508.
34. Fisher, Z., Prada, J. A. H., Tu, C., Duda, D., Yoshioka, C., An, H., Govindamy, L., Silverman, D. N., and McKenna, R. (2005) Structural and Kinetic Characterization of Active-Site Histidine as a Proton Shuttle in Catalysis by Human Carbonic Anhydrase II, *Biochemistry 44*, 1097−1105.
35. Iversen, G., Kharkats, I. Y., and Ulstrup, J. (1998) Simple Dielectric Image Charge Models for Electrostatic Interactions in Metalloproteins, *Mol. Phys. 94*, 297−306.
36. Bashford, D., Karplus, M., and Canters, G. W. (1988) Electrostatic Effects of Charge Perturbations Introduced by Metal Oxidation in Proteins, *J. Mol. Biol. 203*, 507−510.
37. deSilva, D. G. A. H., Beokubetts, D., Kyritsis, P., Govindaraju, K., Powls, R., Tomkinson, N. P., and Sykes, A. G. (1992) Protein Protein Cross-Reactions Involving Plastocyanin, Cytochrome-f and Azurin: Self-Exchange Rate Constant and Related Studies with Inorganic Complexes, *J. Chem. Soc., Dalton Trans. 14*, 2145−2151.
38. McLeod, D. D. N., Freeman, H. C., Harvey, I., Lay, P. A., and Bond, A. M. (1996) Voltammetry of plastocyanin at a graphit electrode: Effects of structure, charge, and electrolyte, *Inorg. Chem. 35*, 7156−7165.
39. Hansen, D. F., Hass, M. A. S., Christensen, H. M., Ulstrup, J., and Led, J. J. (2003) Detection of Short-Lived Transient Protein-Protein Interactions by Intermolecular Nuclear Paramagnetic Relaxation: Plastocyanin from *Anabaena variabilis*, *J. Am. Chem. Soc. 125*, 6858−6859.

BI701446U